DC Signature Analysis Aided Power Source Identification

Rajdeep Choudhury[1,2], Akash Kumar Mandal[1,2], Swades De[1,2], Kaushik Saha[1], and Ranjan K. Mallik[1,2]
[1]Department of Electrical Engineering, [2] Bharti School of Telecommunication Technology and Management
Indian Institute of Technology Delhi, New Delhi 110016, India

***Abstract*—This paper proposes a novel design for identification of input power sources in an electronic system fed through a direct current (DC)-bus powered by multiple input sources. A high-sampling power source identification module is designed to record highly precise DC voltage and current measurements. These measurements are passed through a moving average filter to remove high frequency outliers. A filtered support vector machines approach is proposed for classification of the input source, based on load-end rectified DC signatures. Using a variable sampling rate of up to 1000 samples per second, preliminary laboratory tests demonstrate that the proposed design works with $> 76\%$ gain in accuracy and $> 66\%$ gain in sensitivity over the state-of-the-art support vector machine classifier in 0.5 second of training time and is highly robust to measurement noise.**

***Index Terms*—Harmonic source identification, linear discriminant analysis, moving average filter, support vector machine**

I. Introduction

Most of the power plants generate alternating current (AC) power, while a few generate direct current (DC) power. The DC power is converted into AC and stepped-up for lossless transmission through the power lines. However, the disruption-prone supply of AC power makes it less desirable in providing reliable supply to high-value services and utilities. The unidirectional flow of DC power provides a more reliable alternative for powering electronics and storing power in batteries [1]. Therefore, most electronics utilities, such as enhanced motion vehicles' charging stations, cellular base-stations, and other automated applications, use DC power [2].

In such arrangements, the rectifier is powered by multiple sources to generate reliable DC power for the utility. Power quality from various sources injects different harmonics in the output power, which degrade the performance and lifetime of the load [3]. Furthermore, these harmonics might propagate through various parts of the system, thereby causing damage [4]. Source identification at the DC distribution points is of great interest because of its generalized capability of dealing with any number of sources and the non-intrusive nature of the signal analysis module [5]. Furthermore, such information could help utilities in understanding their billing. However, input source identification from the DC output points is a challenging problem due to 'source masking', where the intermediate rectifier module makes it difficult to identify the input source at the DC (load) end [6]. As the source signatures are flattened and influenced by the rectifier-specific signature, the complexity of input source identification increases further.

A. Literature Review and Motivation

Input power characterization in literature can be broadly put in two sets. The first set [7], [8], [9] undertakes the identification of harmonic source distortion for AC devices using learning-based approaches. The work in [10] proposed islanding detection in power networks using support vector machines (SVMs). A non-intrusive graph signal processing was employed in [11] for load energy disaggregation. However, the non-discrete changes in load power were still difficult to identify. The authors in [12] addressed this issue by realizing the whole classification process with a power spectrum-based wavelet processing. Though these methods provide desirable results in classifying AC signatures, none of these work with DC load signatures, which have become prevalent with rising electronic integration with electrical networks [13]. Furthermore, capturing extreme frequency components of the DC wave requires high sampling devices, which have not been reported with such classification capabilities in literature.

The second set [14], [15] uses signal processing and clustering approaches for identifying harmonic sources in DC pulsed load systems. A short time Fourier transform has been used in [16] for fault identification in DC microgrids, while [17] used long-short term memory networks for fault detection in solar arrays. Though these methods show appreciable performance in harmonic recognition and fault identification in DC systems, they do not consider the problem of input source identification from the DC bus. Such considerations become prevalent when the node is equipped with higher input redundancy to ensure energy sustainability. To deal with such situations, the work in [18] proposed several conditions for harmonic source identification in power networks. However, these conditions are hard to meet for a DC bus system. Thus, none of the existing methods in literature can be used for the classification of input power sources based on the DC load signature.

To summarize, none of the approaches in the literature considered input source identification and the instants of switchover, from the load-end DC measurements. With the rise in the number of electronic loads requiring reliable DC supply, and the use of green energy resources, as in cellular base stations, such scenarios have assumed importance. To this end, this paper proposes a filtered SVM (FSVM) approach for identifying the input power sources based on their remnant signatures after processing by the DC power module. Such processing flattens input source signatures and adds rectifier specific nonlinear harmonics, making the identification

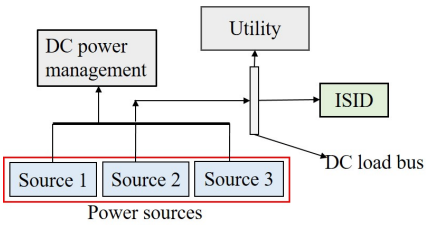

Fig. 1: Powering and monitoring of high-value DC utility.

of sources increasingly difficult. A high-sampling hardware module is designed that records timestamped voltage and current values, and employs FSVM processing to achieve source identification along with the instances of switchovers.

B. Contributions

The key contributions of this work are as follows: 1) A non-invasive high-sampling input source identification device (ISID) is designed. 2) An optimum moving average (MA) filter is employed to filter out high frequency outliers. 3) An FSVM classifier realized by the association of MA-based linear discriminant analysis (LDA)-aided SVM is trained on the labeled data and various source signatures are identified. 4) Optimum hyper-parameters are used for training the FSVM classifier followed by the real-time detection of source switchovers.

Preliminary lab tests demonstrate a sufficiently accurate signature recording and switchover detection using the ISID. The data recording module provides sampling rate of up to 1000 samples per second (sps). The processing module operates with an adaptable training length and filter-lag. In our implementation, 2 lag samples, an optimum training length of 500 samples, and a training time of 0.5 second resulted in 76.47% enhanced accuracy of classification and 66.67% gain in sensitivity. This device can also be used to identify load switchover in AC and DC grids, fault and islanding detection, harmonic identification in pulsed load systems, and classification of disturbance source in smart grid networks.

In the following, Section II gives the system model, Section III discusses the design of the ISID, followed by results and conclusion in Sections IV and V, respectively.

II. System Model for ISID Design

A power-up infrastructure for a high-value utility, such as a cellular base station, is described in Fig. 1. Multiple input sources represented as 'Source i', $i = 1, 2, 3$ (Fig. 1, red box) are fed to the DC power management module, which manages the source switchover and conversion to DC power. The output of the DC power management block is fed to the high value utility through the DC load bus. The DC power management block is tasked with uninterruptible supply to the base station, ensuring reliable network services [19].

The default supply to the DC load bus is maintained through 'Source 1', which in turn also charges an energy storage module (Source 2) to a pre-defined voltage V_0. In the event of failure, the input is immediately switched to a battery source through the power management block. The battery source remains functional until a fraction η discharge is attained, resulting in a cutoff voltage $V_c = \eta V_0$. Once this happens, the source is switched to 'Source 3', which powers the base station and the battery, through the power management block.

The proposed design, shown in the green box of Fig. 1, is used at the DC load bus for high-frequency sampling of DC source signatures, real-time source labeling, and switchover identification. The design of the ISID is described next.

III. Design of ISID

This section explains the construction and working of the ISID including design of the sensing module, the optimal MA filter, and the data analysis module.

A. Design of Sensing Module

The DC input to the cellular base station is monitored using ISID. The sensing module in Fig. 1 consists of voltage and current sensors, threaded parallely to an analog-to-digital converter (ADC). The voltage values are stepped down using a power metal resistive potential divider, and the current is captured using a high-accuracy programmable current sensor. These readings are quantized by the ADC, which provisions programming at a variable sampling rate, based on the source characteristics under observation. These timestamped values are passed to the filtering module. The data analysis module does subsequent processing, and undertakes source classification and switchover identification in real-time.

B. Optimum Filter Design

The timestamped values from the sensing module are passed through the MA filter, which is used to smoothen out noise or remove unwanted fluctuations from the signal. The filter operates by averaging the values of the signal over a sliding window of a fixed length, which moves over the data stream in a time division multiplexed manner. Let the current and voltage values be stored in vectors $\mathbf{x}$ and $\mathbf{y}$, respectively, where x_i, y_i (components of $\mathbf{x}$ and $\mathbf{y}$, respectively), $z_{MA,i}$ represent the input signal values and the desired output of the moving average filter at the i-th instant and N is the length of the moving average window. Further, let us define the transient impedance as $z_i = \frac{y_i}{x_i}$. The moving average filter works by taking the weighted average of the current and previous $N-1$ input values at each time step, given by

$$z_{MA,i} = \sum_{j=i-N+1}^{i} a_j z_j, \tag{1}$$

where $i \geq N-1$ is the filter order and a_j are the filter coefficients. Let κ_i denote the spike impedance given by $\kappa_i = \lim_{\delta \to \epsilon} \frac{z_i - z_{i-\delta}}{\delta}$, where δ is the sampling rate, and ϵ is a small number. The optimization problem is given as

$$\begin{aligned} (\mathbf{P}_1): &\min \sum_{j=1}^{D} |z_{MA,i+j-1} - z_{i+j-1}|^2 \\ \text{s.t. } \mathbf{C}_1: &\ N \in \mathbb{N}, N \geq 1, \\ \mathbf{C}_2: &\ a_1, a_2, \ldots, a_N \in \mathbb{R} \\ \mathbf{C}_3: &\ \sum_{k=1}^{N} a_k = 1, \end{aligned} \tag{2}$$

where the optimization in (2) is solved for D consecutive instants starting from the current i-th instant, $\mathbb{N}$ and $\mathbb{R}$ represent the set of natural and set of real numbers, respectively. The objective function represents the sum of squared differences between the energy of the output of the moving average filter and the recorded signal. The goal is to minimize this difference, which is a measure of the quality of the filter. Constraint $\mathbf{C}_1$ ensures that the filter order is a positive integer, $\mathbf{C}_2$ justifies that the filter coefficients are real numbers, and $\mathbf{C}_3$ ensures that the filter coefficients sum to 1. This is because the moving average filter is a linear filter, and the sum of the coefficients determines the gain of the filter. By constraining the sum of the coefficients to 1, we ensure that the filter does not cause amplification or attenuation effects.

Lemma 1. *The optimal filter of order N and coefficients a_i, s.t. $i \in 1, 2, \cdots, N$, are given by $N = \left\lceil \frac{2D}{\sum_{i=1}^{D}(\kappa_i)^2} \right\rceil$ and $a_k = \frac{\sum_{i=1}^{k}(z_i - z_{MA,i-1})\kappa_{i-k+1}}{\sum_{i=1}^{D}(\kappa_i)^2}$, respectively, where $\lceil \cdot \rceil$ is the ceiling function, z_i is the transient impedance and κ_i is the spike impedance at the i-th instant.*

Proof. See Appendix A. □

From Lemma 1, the optimal filter order N is noted to depend on the signal length, the variance of the input signal, and the sampling frequency through z_i. The filter coefficients a_k are computed using a sliding window of length N over the input and desired output signals, and are normalized by the sum of squares of the input signal.

C. Design of Data Analysis Module

The output of the MA filter is passed to the data analysis module. An LDA-aided SVM is used in real-time processing of this data. This method involves using LDA to transform the original feature space into a lower-dimensional space, followed by SVM to classify the transformed data. Let us assume that we have a dataset containing n samples, where each sample is represented by a vector of p features, denoted by $\mathbf{z}_{MA}^{(r)} = [z_{r1}, z_{r2}, \ldots, z_{rp}]^T$, where T represents the transpose operation, and its corresponding class label L_r, such that $r \in 1, \cdots, M$. The goal is to learn a function that maps the feature space to the class labels. LDA involves transforming the original feature space into a lower-dimensional space that maximizes the separation between the classes. Specifically, LDA seeks to find a linear combination of the features that best separates the classes. Let $\boldsymbol{\mu}_r$ and $\boldsymbol{\Sigma}_r$ be the mean vector and covariance matrix for class r, respectively. The LDA projection vector $\boldsymbol{\omega}_r$ is given by

$$\boldsymbol{\omega}_r = \boldsymbol{\Sigma}^{-1} \left(\boldsymbol{\mu}_{\text{ref}} - \boldsymbol{\mu}_r \right), \tag{3}$$

where $\boldsymbol{\mu}_{\text{ref}}$ is the mean of the reference class which can be chosen randomly from the existing M classes, $\boldsymbol{\Sigma}$ is the pooled in-class covariance matrix given by

$$\boldsymbol{\Sigma} = \frac{\sum_{r=1}^{M}(n_r - 1)\boldsymbol{\Sigma_r}}{\sum_{r=1}^{M} n_r - M}, \tag{4}$$

Algorithm 1 FSVM Algorithm

1: Read signal data from source
2: Apply optimum MA filter to remove noise
3: Normalize the data to ensure consistency
4: Split the processed data into training and test set
5: Scale the features to achieve zero mean and unit variance
6: Train the model using LDA+SVM on the training set
7: Use the trained model to predict outcomes on the test set
8: Construct the confusion matrix to evaluate performance
9: Compute accuracy, precision, and Recall for each category

where n_r is the number of observations in the r-th class. Thus, the transformed feature space is given by

$$z_{F,r} = \boldsymbol{\omega}_r^T \mathbf{z}_{MA}^{(r)}, \tag{5}$$

where $z_{F,r}$ is the r-th transformed feature and $\boldsymbol{\omega}_r$ is a $p \times 1$ vector, where p is the number of features in the original feature space. Given the transformed data $z_{F,r}$ and their corresponding class labels L_r, SVM seeks to find the hyperplane, which is a 1-dimensional line in this case, is expressed as

$$w z_{F,r} + b = 0, \tag{6}$$

where w is the weight and b is the bias term. The weight w in (6) operates on the transformed feature $z_{F,r}$. The optimal hyperplane is determined as [20]

$$\begin{aligned} (\mathbf{P}_2): \ & \min_{w,b} \frac{1}{2}|w|^2 + \gamma \sum_{r=1}^{M} \xi_r \\ \text{s.t. } \mathbf{C}_4: \ & L_r(w z_{F,r} + b) \geq 1 - \xi_r \\ \mathbf{C}_5: \ & \xi_r \geq 0, \ r = 1, 2, \cdots, M, \end{aligned} \tag{7}$$

where γ is a regularization parameter that balances the trade-off between maximizing the margin and minimizing the classification error, and ξ_r are slack variables that allow for some mis-classification. The SVM solution involves finding the weight w and bias term b that minimize the above objective function subject to the constraints. Once the SVM has been trained on the transformed data, it is used to classify new samples by transforming them using the same projection w and evaluating the SVM decision function [21]

$$\hat{y}_r = \text{sgn}(w z_{F,r} + b), \tag{8}$$

where sgn is the signum function and $\hat{L}_r$ is the predicted class label for the r-th class. The SVM solution involves finding the weight w and bias term b that maximize the margin between the classes, subject to the constraints. To solve the SVM optimization problem, we use the Lagrange dual formulation, which involves finding the Lagrange multipliers α_r that satisfy the Karush-Kuhn-Tucker conditions. The optimal weight and bias term are given by [22]

$$w = \sum_{r=1}^{M} \alpha_r L_r z_{F,r}; \, b = \frac{1}{N_s} \sum_{r_1=1}^{M} \left(L_{r_1} - \sum_{r_2=1}^{M} \alpha_{r_2} L_{r_2} z_{F,r_2} z_{F,r_1} \right), \tag{9}$$

where N_s is the number of support vectors. The detailed procedure for source classification and identification of switchover is outlined in Algorithm 1. The proof of convergence for the FSVM algorithm is done in the following paragraph.

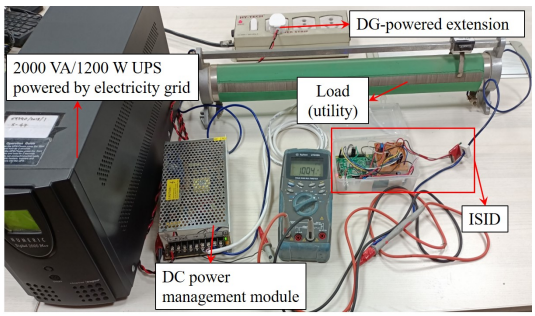

Fig. 2: Laboratory test setup for ISID based source identification.

Lemma 2. *The FSVM algorithm converges in finite time.*

Proof. See Appendix B. □

IV. Results and Discussion

This section presents performance results on the proposed ISID design. The proposed hardware is specified in terms of high-sampling DC signature recording, while the analysis module is contrasted with the state-of-the-art classification frameworks, such as, decision tree and SVM, in terms of the key performance indices (KPIs).

Construction of dataset: The data is captured using the ISID hardware on a 54 V, 1 A DC load fed by the grid, a 2000 VA/1200 W battery, and a generator. The ISID is operated for 30 minutes, during which natural switchovers are recorded and identified. Performance comparison and preliminary test results on the setup in Fig. 2 are presented in subsequent subsections. The dataset and code are uploaded at https://github.com/AakashKumarMandal/ISID.

A. Key Performance Indices

The following are the KPIs used in establishing the performance of the proposed data analysis algorithm.

1) Accuracy: The accuracy ζ is defined as the fraction of correct predictions (ζ_C) out of the total number of predictions (ζ_T). Mathematically, we have $\zeta = \frac{\zeta_C}{\zeta_T}$.

2) Precision: The precision ϕ is defined as the ability of the classification model in identifying the observations correctly within the class. Let there be τ^+ and $\overline{\tau}^+$ true positives and false positives, respectively. The precision $\phi = \frac{\tau^+}{\tau^+ + \overline{\tau}^+}$.

3) Sensitivity: The sensitivity is defined as the ability of the model to repeatedly predict a particular class correctly. Let τ^+ and τ^- represent the number of true positive and false negative classifications made by the classification model. Then, mathematically we have $\theta = \frac{\tau^+}{\tau^+ + \tau^-}$.

Performance analysis using these KPIs is presented next.

B. Optimal Hyper-Parameter Selection

Fig. 3 describes the optimal choice of hyper-parameters for the FSVM algorithm (c.f. Algorithm 1). From Fig. 3(a) we observe that with the increase in training length, the precision attained by the FSVM algorithm increases to a maximum, then either saturates or decreases, based on the sampling frequency. This is a result of over-training of the FSVM algorithm at higher training lengths. Also, from Fig. 3(a), we note that an optimum training length of 500 samples at a sampling rate of 700 sps leads to ≥ 0.99 precision.

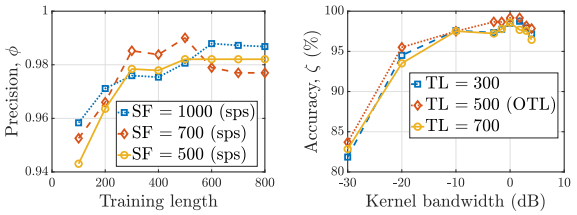

(a) (b)

Fig. 3: (a) Precision versus training length at $\gamma = 1.5$ and (b) accuracy versus bandwidth of kernel function.

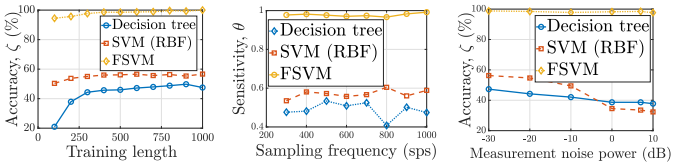

(a) (b) (c)

Fig. 4: (a) Accuracy versus training length at sampling frequency of 1000 sps; (b) sensitivity versus sampling frequency at training length of 500 samples; (c) accuracy versus measurement noise at training length of 500 samples, and $\gamma = 1.5$.

In Fig. 3(b), we note that the classification accuracy increases with the increase in kernel bandwidth of the radial basis function corresponding to all training lengths. As expected, it is notable that at the optimal training length of 500 samples, 100% accuracy is attained at $\gamma \approx 1.5$. A slight drop in classification accuracy is notable around this kernel bandwidth. Therefore, from Fig. 3(b) we observe that the proposed classification algorithm performs best at a kernel bandwidth $\gamma \approx 1.5$, resulting in a classification accuracy of $\approx 99.2\%$. During our simulation, we found the best performance for the FSVM algorithm at an optimum lag length of 2 samples with the filter coefficients given by [0.7, 0.3].

C. Performance Comparison of ISID

Fig. 4 demonstrates the performance of the proposed algorithm with the state-of-the-art classification algorithms with the KPIs listed in subsection IV-A. From Fig. 4(a), we note that for all the classification approaches, the accuracy increases with the increase in training length. However, as a consequence of optimal data filtering, the proposed algorithm reaches $\approx$ 100% accuracy in 500 training samples, which correspond to ≈ 0.5 second of recorded data at 1000 sps. Thus, we conclude that the proposed module achieves optimum performance in a low fraction of time. From Fig. 4(a), we find a 76.47% gain in the accuracy of classification. As a result, the points of switchovers were identified with a high degree of accuracy, as described in the next subsection.

From Fig. 4(b), we note that the proposed algorithm works with close to unit sensitivity, which implies that the proposed design is able to repeatedly classify the points in the correct classes with high accuracy. This accuracy increases with the sampling frequency, resulting from the model training being done on more data points. Further, it is notable that all the

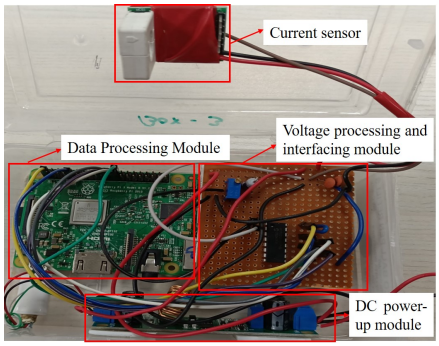

Fig. 5: Design of ISID.

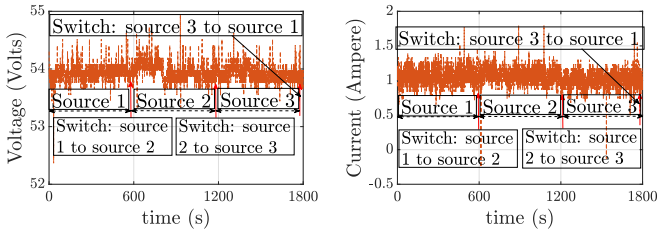

(a) (b)

Fig. 6: Source classification and switchover identification: (a) voltage and (b) current measurements; Source 1/2/3: grid/battery/generator.

other state-of-the-art algorithms operate below 0.6 sensitivity. This is mainly a consequence of the flattened DC signatures at the output end of the DC power management module. Since, the proposed algorithm uses MA filtering, the relevant features are appropriately identified, leading to an improved performance in source classification. On a comparative analysis, we find 66.67% gain in sensitivity over the state-of-the-art.

Fig. 4 demonstrates a comparative study on the robustness of the proposed design in source classification with the state-of-the-art classification approaches. As can be expected, the performance of decision tree and SVM classifiers degrades massively, as the noise in the measurement data increases. It is noteworthy that this degradation is by the virtue of absence of any finite impulse response filter. Since, the proposed FSVM approach employs an MA filter, we note that the proposed classifier is fairly robust to the increase in noise power, and operates with accuracy close to 100%. Therefore, from Fig. 4, we conclude that the proposed ISID gives a very accurate and robust handle at classifying the input sources of power based on the load-end DC signature.

Remark 1. *It is noteworthy that, the proposed FSVM classifier benefits from the use of MA filter, which processes the DC data to gather relevant source-specific signatures. This is a major contributor in the high achieved source switchover accuracy and precision by the proposed ISID design.*

D. Construction and Lab Testing of ISID

Fig. 5 depicts the design of the ISID used in input source identification using the load-end DC signature. The proposed design consists of the DC power-up module (EC-6635), voltage processing and interfacing module, current sensor module (WCS6800), and data processing module. The DC power-up module taps the input voltage level to power the current sensing and data processing modules. The non-invasive current sensor and voltage processing module are interfaced through the high-sampling ADC (MCP3208) with the data processing module. The data processing module is tasked with the implementation of an MA filter, and the FSVM approach is used for accurate detection of the sources in run-time and for identification of source switch-overs.

Fig. 6 demonstrates the results depicting the performance of the proposed design under field test. Real switching scenarios between grid, battery, and generator are created and the proposed design is deployed to detect the input power sources and identify the switchovers. It is observed from the voltage and current signatures depicted in Figs. 6(a) and (b), respectively, that the source switchovers are accurately identified (depicted by the red arrow at the junction of consecutive double-headed arrows) in both the voltage and current measurements, as outlined by the accuracy results in Fig. 4(a), in real-time. Therefore, we conclude that the proposed ISID demonstrates promising performance results in our preliminary lab tests with a high classification accuracy.

Remark 2. *The input source parameters, such as voltage, frequency, or duration of operation do not impact the accuracy of the algorithm. This is a consequence of the FSVM algorithm being agnostic to the voltage level and the wide operation frequency range of the sensors. Furthermore, the algorithm was tested with various source operation duration and switchover instants. Since the framework does not need any prior information of the source signatures, the timing of the input sources was noted to play no role in the process.*

V. Concluding Remarks

This paper proposed a novel design of an ISID for high accuracy detection of input power sources based on the load-end DC signature. An FSVM classification methodology was proposed for highly precise identification of source switchovers. Optimal hyper-parameters were chosen based on the signature profile of the DC load voltage and current measurements. The proposed ISID design was noted to achieve a significantly improved accuracy, sensitivity, and precision in input power source classification over the state-of-the art harmonic source identifiers. Moreover, the classification was achieved in fairly less time compared to the existing state-of-the-art classification approaches. Further, it was noted that the proposed module renders robust performance under varying order of measurement noise power, which is especially relevant considering the noisy industrial data measurement environment. Preliminary lab tests corroborated the accuracy and robustness of the proposed ISID. In future, we plan to make this a part of industrial Internet-of-Things network by adding a smart communication module in the proposed design.

Acknowledgement

This work was supported in parts by the Indian National Academy of Engineering (INAE) through the Abdul Kalam Technology Innovation National Fellowship and Prime Minister's Doctoral Research Fellowship.

APPENDIX

A. Proof of Lemma 1

The optimization problem $(\mathbf{P}_1)$ is solved by the method of Lagrange multipliers. The Lagrangian $\mathscr{L}(\cdot)$ is given as

$$\begin{aligned}\mathscr{L}\left(N, a_k, \lambda_1, \lambda_2\right) =& \sum_{j=1}^{D} \left|z_{MA,i+j-1} - z_{i+j-1}\right|^2 \\ &+ \lambda_1 \left(N-1\right) + \lambda_2 \left(\sum_{k=1}^{N} a_k - 1\right),\end{aligned} \tag{A1}$$

where λ_1 and λ_2 are Lagrange multipliers that enforce the constraints on the filter order and coefficients. We take the partial derivatives of the Lagrangian with respect to the filter coefficients and Lagrange multipliers, and set them to zero. This results in $\frac{\partial L}{\partial a_k} = 0$, $\frac{\partial L}{\partial \lambda_1} = 0$, and $\frac{\partial L}{\partial \lambda_2} = 0$. Solving the first two equalities, we obtain

$$\begin{aligned}\lambda_1 &= 2\sum_{j=1}^{D} (z_{MA,i+j-1} - z_{i+j-1})\kappa_{i+j-N}, \\ \text{and } \lambda_2 &= 2\sum_{k=1}^{N} a_k - 2.\end{aligned} \tag{A2}$$

Substituting these expressions in the last equality we get

$$N - 1 - \sum_{k=1}^{N} a_k = 0 \; ; \; \sum_{k=1}^{N} a_k - 1 = 0. \tag{A3}$$

Solving (A3), we get $N = \left\lceil \frac{2D}{\sum_{i=1}^{D}(\kappa_i)^2} \right\rceil$ and $a_k = \sum_{i=1}^{k}(z_i - z_{MA,i-1})\kappa_{i-k+1} \left(\sum_{i=1}^{D}(\kappa_i)^2\right)^{-1}$.

B. Proof of Lemma 2

We divide the convergence analysis for the FSVM algorithm into proving three consecutive convergences, for the MA filter, LDA, and SVM. From the filter structure in (1), we note that the filter is bounded-input-bounded-output stable. Therefore, since the energy of the input signal is bounded, the filter output converges with uniqueness. Next, the convergence of LDA depends upon the structure of the optimization problems in (2). Let us denote the function inside the summation as $\mathscr{P}(z_{MA,i}, z_i) = |z_{MA,i} - z_i|^2$. Since, $\mathscr{P}(\cdot)$ is a combination of two smooth functions, namely the Euclidean norm and the square function, we conclude that it is smooth. Further, using the reverse triangle inequality, we establish $0 \leq \mathscr{P}(z_{MA,i}, z_i) \leq |z_{MA,i}|^2 + |z_i|^2$. As the optimization function is both smooth, bounded, and convex, we establish the convergence of LDA [23]. Similarly, based on (7), we conclude that the SVM algorithm converges to a unique optimum. Therefore, we conclude that the FSVM is convergent.

REFERENCES

[1] L. He, Y. Li, Z. Shuai, J. M. Guerrero, Y. Cao, M. Wen, W. Wang, and J. Shi, "A flexible power control strategy for hybrid AC/DC zones of shipboard power system with distributed energy storages," *IEEE Trans. Indus. Informat.*, vol. 14, no. 12, pp. 5496–5508, 2018.

[2] M. R. Khalid, I. A. Khan, S. Hameed, M. S. J. Asghar, and J.-S. Ro, "A comprehensive review on structural topologies, power levels, energy storage systems, and standards for electric vehicle charging stations and their impacts on grid," *IEEE Access*, vol. 9, pp. 128 069–128 094, 2021.

[3] Y. He, H. S.-H. Chung, C.-T. Lai, X. Zhang, and W. Wu, "Active cancelation of equivalent grid impedance for improving stability and injected power quality of grid-connected inverter under variable grid condition," *IEEE Trans. Power Electron.*, vol. 33, no. 11, pp. 9387–9398, 2018.

[4] A. K. Mandal, A. Malkhandi, S. De, N. Senroy, and S. Mishra, "A multipath model for disturbance propagation in electrical power networks," *IEEE Trans. Circuits Syst. II: Express Briefs*, vol. 70, no. 4, pp. 1460–1464, 2023.

[5] Y. Shan, J. Hu, K. W. Chan, Q. Fu, and J. M. Guerrero, "Model predictive control of bidirectional DC–DC converters and AC/DC interlinking converters—A new control method for PV-wind-battery microgrids," *IEEE Trans. Sustain. Ener.*, vol. 10, no. 4, pp. 1823–1833, 2018.

[6] S. Beheshtaein, R. M. Cuzner, M. Forouzesh, M. Savaghebi, and J. M. Guerrero, "DC microgrid protection: A comprehensive review," *IEEE J. Emer. Selec. Topics Power Elec.*, pp. 1–1, 2019.

[7] D. Srinivasan, W. Ng, and A. Liew, "Neural-network-based signature recognition for harmonic source identification," *IEEE Trans. Power Deliv.*, vol. 21, no. 1, pp. 398–405, 2006.

[8] H.-H. Chang, K.-L. Chen, Y.-P. Tsai, and W.-J. Lee, "A new measurement method for power signatures of nonintrusive demand monitoring and load identification," *IEEE Trans. Indus. Appl.*, vol. 48, no. 2, pp. 764–771, 2012.

[9] T.-T.-H. Le, H. Kang, and H. Kim, "Household appliance classification using lower odd-numbered harmonics and the bagging decision tree," *IEEE Access*, vol. 8, pp. 55 937–55 952, 2020.

[10] B. Matic-Cuka and M. Kezunovic, "Islanding detection for inverter-based distributed generation using support vector machine method," *IEEE Trans. Smart Grid*, vol. 5, no. 6, pp. 2676–2686, 2014.

[11] K. He, L. Stankovic, J. Liao, and V. Stankovic, "Non-intrusive load disaggregation using graph signal processing," *IEEE Trans. Smart Grid*, vol. 9, no. 3, pp. 1739–1747, 2018.

[12] H.-H. Chang, K.-L. Lian, Y.-C. Su, and W.-J. Lee, "Power-spectrum-based wavelet transform for nonintrusive demand monitoring and load identification," *IEEE Trans. Indus. Appl.*, vol. 50, no. 3, pp. 2081–2089, 2014.

[13] E. A. M. Ceseña and P. Mancarella, "Energy systems integration in smart districts: robust optimisation of multi-energy flows in integrated electricity, heat and gas networks," *IEEE Trans. Smart Grid*, vol. 10, no. 1, pp. 1122–1131, 2018.

[14] Y. Ma, A. Maqsood, D. Oslebo, and K. Corzine, "Wavelet transform data-driven machine learning-based real-time fault detection for naval DC pulsating loads," *IEEE Trans. Transport. Electrific.*, vol. 8, no. 2, pp. 1956–1965, 2022.

[15] P. Pietrzak and M. Wolkiewicz, "On-line detection and classification of PMSM stator winding faults based on stator current symmetrical components analysis and the KNN algorithm," *Electronics*, vol. 10, no. 15, 2021. [Online]. Available: https://www.mdpi.com/2079-9292/10/15/1786

[16] A. Maqsood, D. Oslebo, K. Corzine, L. Parsa, and Y. Ma, "STFT cluster analysis for DC pulsed load monitoring and fault detection on naval shipboard power systems," *IEEE Trans. Transport. Electrific.*, vol. 6, no. 2, pp. 821–831, 2020.

[17] A. Y. Jaen-Cuellar, D. A. Elvira-Ortiz, R. A. Osornio-Rios, and J. A. Antonino-Daviu, "Advances in fault condition monitoring for solar photovoltaic and wind turbine energy generation: A review," *Energies*, vol. 15, no. 15, 2022. [Online]. Available: https://www.mdpi.com/1996-1073/15/15/5404

[18] B. Wang, G. Ma, J. Xiong, H. Zhang, L. Zhang, and Z. Li, "Several sufficient conditions for harmonic source identification in power systems," *IEEE Trans. Power Deliv.*, vol. 33, no. 6, pp. 3105–3113, 2018.

[19] *Management Discussion and Analysis-Integrated Report and Annual Financial Statements*, Bharti Airtel Limited, 2018-19. [Online]. Available: https://www.airtel.in/airtel-annual-report-2018-19/pdf/MDA.pdf

[20] S. Tripathi and S. De, "Dynamic prediction of powerline frequency for wide area monitoring and control," *IEEE Trans. Indus. Informat.*, vol. 14, no. 7, pp. 2837–2846, 2017.

[21] R. Gupta, V. Gupta, A. K. Mandal, and S. De, "Learning-based multivariate real-time data pruning for smart PMU communication," in *2022 IEEE 19th Annual Cons. Commun. Netw. Conf. (CCNC)*, Las Vegas, NV, USA, 2022, pp. 326–331.

[22] N. Cristianini, J. Shawe-Taylor, *An Introduction to Support Vector Machines and Other Kernel-Based Learning Methods*. Cambridge, UK: Cambridge University Press, 2000.

[23] S. Boyd and L. Vandenberghe, *Convex Optimization*. Cambridge, UK: Cambridge University Press, 2004.